An Experimental Study of Turbulent Mixing in a Tee Mixer Using PIV and PLIF

Gang Pan and Hui Meng

Laser Flow diagnostics Laboratory, Dept. of Mechanical & Aerospace Engineering,

State University of New York at Buffalo, Buffalo, NY 14260

Turbulent scalar mixing in the near field of a tee mixer (transverse jet in a pipe) is

studied using Particle Image Velocimetry (PIV) and Planar Laser Induced Fluorescence

(PLIF). Two jet-to-pipe velocity ratios, r = 3.06 and r = 5.04, are investigated for a

turbulent pipe flow at a Reynolds number of 20,850. The laser measurement techniques

are described, typical flow structures in the near field of tee mixer are examined, and

turbulence statistics and scalar statistics are calculated. The general behavior of mixing

is analyzed from the jet expansion and the concentration decay along the jet centerline,

and the flow condition for jet impingement on the pipe wall is estimated. The mixing

mechanism in the near field is revealed from the variation of the scalar PDF across the

jet. Results suggest that the mixing on the upstream side of the jet is dominated by large-

scale structures and on the downstream side by small eddies and turbulent diffusion,

where the β -PDF is an excellent approximation.

Topical Area: Fluid Mechanics and Transport Phenomena

Key Words: Turbulent mixing, jet mixing, tee mixer, PIV, PLIF, β -PDF

1 Introduction

In the chemical process industry turbulent jets are widely used for mixing miscible liquids. A

common configuration of turbulent jet mixer for efficiently mixing two rapidly reacting fluids is

the jet in a confined crossflow (which can be a pipe flow or a duct flow) known as the tee mixer

or the side-entry mixer. In a basic tee mixer configuration a fast-moving turbulent jet flow is

injected radially into a fully developed turbulent pipe flow with the goal of quickly destroying the

spatial inhomogeneity relative to the characteristic reaction time. Since the maximal yields of the

desired chemical products are obtained when the reactions take place in a homogenous scalar

field, and in fast reaction cases the product quality is strongly affected by the non-homogeneity of

Correspondence concerning this article should be addressed to H. Meng (Email: huimeng@eng.buffalo.edu).

1

the reactants, the faster the homogeneity is achieved through mixing the better the mixer. It is thus the goal of mixer design to find the optimal geometries and flow conditions in a tee mixer to rapidly achieve a homogeneous scalar field.

In turbulent scalar mixing of non-premixed fluids segregation is often used to quantify the goodness of mixing. Turbulent dispersion (macromixing) controlled by the energy-containing large-scale eddies works to decrease the scale of segregation while at small scales molecular diffusion (micromixing) acts to decrease the intensity of segregation to achieve the ultimate mixing before chemical reaction can take place (Brodkey, 1967). In a tee mixer turbulent dispersion dominates the near field (i.e. x < 2D, where D is the pipe diameter) where the energetic eddies exist and molecular diffusion is most significant in the far field (i.e. x > 3D) where the scale of segregation is sufficiently small.

The objective of this research is to carry out a relatively detailed experimental study of turbulent scalar mixing in the near-field region of a tee mixer using full-field laser-based non-intrusive experimental techniques. We seek to provide the means for acquiring experimental data needed for validating Computational Fluid Dynamics (CFD) in this complex geometry. We focus on the near-field region of the tee mixer not only because it is critical for rapid chemical reaction, but also because the turbulent flow in this region deviates greatly from the homogeneous and isotropic flow assumptions employed by common turbulence models in CFD.

1.1 Review of previous experimental studies

From the fluid dynamics point of view the tee mixer resembles the jet in a crossflow except that the crossflow here is confined in a pipe. Numerous experimental studies have been performed to investigate the vortex dynamics and their influence on mixing in the jet in an unconfined crossflow. Some of the important work includes Fric and Roshko (1994), Kelso et al. (1996), and Smith and Mungal (1998).

In the application areas of mixing and chemical reaction a number of experimental studies have been conducted for the tee mixer using either liquid or gaseous working fluid. Forney and Kwon (1979) measured the jet fluid concentration using a methane tracer with a flame ionization detector (FID) to determine the optimum jet-to-pipe velocity ratio for geometrically centered jets. Maruyama et al. (1981) mixed hot and cold gas streams in the tee mixer and measured the temperature standard deviation as an indication of the degree of mixing. Gosman and Simitovic (1986) used ethylene and FID to study the mixing in a rectangular duct for different injection angles and jet-to-crossflow velocity ratios. They found that the degree of mixing increases with increasing injection angle (from pointing downstream to pointing upstream) and increasing

velocity ratio. Tosun (1987) studied the micromixing in tee mixers by using the azo-coupling reactions to quantify the intensity of micromixing and found that the optimum jet-to-pipe velocity ratio for micromixing is larger than that for macromixing. Cozewith and Busko (1989) studied the mixing of tee mixer by measuring the indicator color region in HCL/NaOH neutralizations as a function of the jet-to-pipe velocity ratio and diameter ratio. They confirmed that centering the jet flow in the main pipe is correlated with the optimal macromixing. They also conducted experiments at different pipe Reynolds numbers of the pipe and found that the mixing is independent of the Reynolds number when the Reynolds numbers is 10,000 or greater. Sroka and Forney (1989) used FID and hot wire to measure both concentration and velocity in a gaseous tee mixer flow. Their results showed that the mean concentration decays as $x^{-2/3}$ and the second moment decays as $x^{-3/4}$ in the near field. Catalano et al. (1991) measured the streamwise velocity in a jet in confined crossflow (gaseous) and computed high-order statistics of the velocity and their time derivatives. They investigated the existence of the universal similarity and constructed the normalized spectra of energy content, dissipation, and higher-order moments in order to examine the Reynolds number dependence of these functions. Hatch et al. (1995) studied the influences of the geometry and the flow on the jet mixing in a pipe by measuring the temperature downstream of a row of cold jets injected into a heated cross-stream. Their results showed that at a fixed momentum-flux ratio, jet penetration decreases with an increase in the aspect ratio or the injection angle with respect to the crossflow direction.

A limitation to most of the previous experimental studies of the tee mixer is that they are based either on intrusive single-point measurements or qualitative flow visualization. Although a number of geometries have been examined, it is impossible to exhaust all possible cases experimentally. The process engineer must therefore resort to CFD simulations for mixer design and analysis, which allow them to "experiment" with a wide range of design options at a relatively low cost and a short turnover time. However, the CFD codes must be validated against detailed experimental data before one can confidently scale up the results. The tee mixer is a complex flow for which the existing CFD models are known to have difficulties in accurately predicting the scalar mixing. Model improvements will depend on the availability of detailed non-intrusive full-field velocity and scalar field measurements. Hence, for CFD validation and improvements, it is important to develop tools for such measurements.

1.2 Present work

The current study uses Particle Image Velocimetry (PIV) and Planar Laser Induced Fluorescence (PLIF) techniques to measure the velocity and concentration fields of the flow in

the tee mixer. The PIV technique has matured over the past decade for measuring two-dimensional velocity fields with relatively high spatial resolution and accuracy (Westerweel, 1997), while PLIF has been demonstrated to be effective of providing planar concentration measurements in both gaseous and liquid flows (Koochesfahani and Dimotakis, 1985, Dahm et al., 1990, Karasso and Mungal, 1996, Unger and Muzino, 1999). However, these techniques have yet to be introduced to the study of tee mixers and the present work starts off this effort. Although at this stage no attempt has been made to actually validate CFD simulations using the measurement results, the initial application of these experimental techniques to the tee mixer has already revealed the great potential of such measurements. Direct observations of our experimental data provide new understandings of the tee mixer, which will be discussed in this paper.

The tee mixer used in the experiment consists of a round turbulent jet (d=1.27cm) injected radially into a turbulent pipe crossflow (D=7.62cm). Both flows are liquid with no chemical reaction. The measurements were carried out for two jet-to-pipe velocity ratios, r, ($r = U_j / U_p$, where U_j is the jet velocity and U_p the pipe velocity) at two perpendicular center planes of the pipe including one that contains the centerline of the side jet.

The paper is organized in the following way: first the experimental facility and the measurement techniques are introduced, then the velocity and concentration results obtained from PIV and PLIF measurements are presented. After that the flow structures in tee mixer flow are examined followed by a discussion of jet characteristics including: parametric length scales, jet centerline concentration decay, jet impingement and jet expansion. Finally, an analysis of the mixing mechanism based on the scalar probability density function (PDF) is given along with the validation of the β-PDF model for binary mixing using the experimental data.

2 Experimental Setup

2.1 Flow facility

Figure 1 is a schematic of the tee mixer flow apparatus. The pipe is a round glass tube 7.62cm in diameter and the water flow is driven through the pipe by a 1.5kW centrifugal pump. The entry arrangement of the pipe flow consists of a settling chamber, a straighten bundle and a diffuser. The flow rate is controlled via a frequency modulator and the maximum Reynolds number based on pipe diameter that can be achieved is Re = 41,680. The jet flow is provided by an overflow reservoir system. It is injected into the pipe radially through a 1.27cm diameter pipe at a position

that is 10 pipe diameters downstream from the pipe entrance. To reduce the optical distortion a rectangular water chamber is installed around the pipe to cover the entire test section.

2.2 PIV setup

Particle Image Velocimetry uses small neutrally buoyant particles as flow tracers to map out flow velocity fields. In this study an in-house developed PIV system was used to measure the turbulent flow in the near field of the tee mixer. The particle-seeded flow is illuminated by a light sheet consisting of a series of laser pulse pairs produced by a pair of Nd:YAG lasers (New Wave MiniLaser, 25mJ per pulse). A digital CCD camera (Kodak ES 1.0) captures time-series images of the particles in the light sheet. The displacement of particles over the double-pulse interval is then computed from the image pair for every interrogation cell using the image-processing program. Since the double-pulse time interval is known, the velocity can be inferred from the displacement. The resultant 2D velocity vector is attributed to a grid point on the imaging plane. After the whole plane is processed an instantaneous 2D velocity field is obtained. In this experiment we employed an interrogation cell of 32×32 pixels (which was a sub-domain of the 992×1008 pixel viewing area). The interrogation cell was shifted with 50% overlap so that 64×64 vectors were produced in each instantaneous PIV sample.

2.3 PLIF setup

The Planar Laser Induced Fluorescence technique measures the planar distribution of the concentration of a fluorescence-producing species, which can be fluorescent dye premixed with a fluid. When a laser sheet illuminates a dye-contained liquid flow, the dye absorbs the laser energy and emits fluorescence at a longer wavelength than the excitation laser light. In the weak excitation range the fluorescence intensity, I_f , is proportional to the local dye concentration C_{dye} as

$$I_f = \eta \cdot \Phi \cdot I \cdot C_{dye} \tag{1}$$

where η is the efficiency of the collection optics, Φ is the effective quantum yield, and I is the local laser intensity. When η , Φ , and I are either known at every point or eliminated from the equation by a ratiometric method, the instantaneous concentration field $C_{dye}(x, y)$ and hence the concentration can be obtained by processing the fluorescence images $I_f(x, y)$.

In the PLIF measurements the setup of optics and imaging was similar to that used in the PIV measurements. To increase the dynamic range of the scalar measurement, a 12-bit cooled digital CCD camera (PCO Sensicam) was employed to record the fluorescence images. To eliminate the overlapping effect of illumination and emission, a narrow band optical filter (550nm \pm 5nm),

which passes the fluorescence wavelength, was placed in front of the camera lens during PLIF image acquisition. A diluted sodium fluorescein solution was used in the PLIF experiment to measure the turbulent mixing. Although the dye solution can be either the jet fluid or the pipe fluid, for convenience of use of the quasi ratiometric method to be described below and for recirculating the pipe flow with minimal dye concentration variation at the inlet of the test section, we chose the dye solution to be the pipe fluid.

Quantitative PLIF measurements requires that the fluorescence emission I_f be linear with the laser intensity I at a given dye concentration, as shown in Eq. (1). This linearity can be verified via the laser attenuation with distance in the dye. Details of the linearity verification are given in the Appendix. With the linear response being obtained, we could use Beer's law to correct the non-uniformity of laser illumination caused by dye absorption. The non-uniformity of laser illumination caused by other factors such as a Gaussian intensity profile of laser, light sheet expansion, and imperfection in the optical elements was corrected by using a quasi ratiometric scheme in which the mixing images were normalized by pre-mixing images recorded under a uniform dye concentration. Other systematic errors such as background illumination and CCD dark noise were removed by subtracting the background images that were acquired in the absence of laser illumination and dye but with the same camera and ambient environment as in the measurements of mixing.

Based on Eq. (1) and the image correction scheme described above, the equation for calculating the concentration of the jet fluid is

$$\xi_n = 1 - \frac{I_n - B_n}{P_n - B_n} \cdot \exp\left\{ -\kappa \cdot C_{dye,I} \cdot \Delta y \cdot \sum_{i=0}^{n-1} \xi_i \right\},\tag{2}$$

where ξ denotes the jet concentration, I, B, P are the gray level of the PLIF images, the background images, and the pre-mixing images respectively, the subscript n denotes the nth pixel of a line in the CCD sensor along the direction of laser propagation, κ is the absorption coefficient of sodium fluorescein, $C_{dye,I}$ is the initial dye concentration in the pipe flow, and Δy is the pixel size of the CCD sensor. The exponential term in the equation results from the Beer's law correction of the dye absorption, and the product $\kappa C_{dye,I}$ can be measured from the pre-mixing reference images by $\kappa C_{dye,I} = (n\Delta y)^{-1} \cdot \ln(I_n/I_0)$.

3 Measurement Description

The flow conditions of the test runs are given in Table 1. Two velocity ratios, r=3.06 and r=5.04, were tested, where the jet exit velocity was varied and the pipe flow rate was kept constant. PLIF data were taken for both cases, while PIV data were taken only for r=3.06. For the PIV measurement the entire flow was seeded with particles and the pipe flow was re-circulated. For the PLIF measurement the pipe flow was premixed uniformly with the dye (0.1mol/m^3) and was re-circulated during the test runs. To ensure the convergence of the statistics of the velocity and concentration fields, 800 PIV image pairs and 500 PLIF images were taken for the PIV and PLIF measurements, respectively.

PIV and PLIF images were taken on two image planes: the side-view plane (x-y plane) at the center of the jet and the top-view plane (x-z plane) at the center of the pipe. The side-view image area for PLIF was $10.2 \text{cm} \times 8.1 \text{cm}$ and extended from x = -d to x = 7d, while that for PIV was $7.6 \text{cm} \times 7.6 \text{cm}$ and extended from x = 0.2d to x = 6.2d. The top-view image plane for both PLIF and PIV ($6.5 \text{cm} \times 8.1 \text{cm}$) extended from x = 0.5d to x = 5.6d. In either view, the imaging window covered the whole pipe diameter in the y or z directions.

The spatial resolution of the measurement was 1.2mm for the velocity field (grid spacing of 64 \times 64 grids) and about 0.5mm for the scalar field (the sheet thickness in PLIF measurement). On the other hand, the Kolmogorov length scale was estimated to be $10\mu m$ based on the jet diameter as the integral length scales, and the Batchelor scale was about 30 times smaller than the Kolmogorov length scale. Therefore, the measurements did not resolve the smallest scales of the flow. Although we could have zoomed in the measurement windows to increase the spatial resolution, it was decided that at this point it was more important to cover the entire pipe diameter for a global assessment of the mixing in the near field of the tee mixer than resolving the fine scales.

The accuracy of PIV measurements ultimately depends on the uncertainty of the measurements of particle displacement. If a standard cross-correlation-based sub-pixel PIV processing technique is used and the valid correlation peaks are detected, a commonly accepted uncertainty in the displacement measurement is 0.1pixel (Keane and Adrian, 1992). In the current measurement we optimized the particle image size (around 4 pixels), particle seeding densities (50~60 particle/mm³), and time interval between two exposures (0.5ms) to secure valid detection of the correlation peak. Under these conditions the uncertainty in velocity measurement can be estimated based on a displacement uncertainty of 0.1pixel. With the double-pulse separation of

0.5ms, 0.1pixel translates to an error of 1.51cm/s in velocity, which was 5.5% of the pipe entry velocity.

As described earlier, in our PLIF technique the systematic errors in the raw images such as background light, CCD sensor dark noise, non-uniform illumination and laser pulse variation were removed before computing the real scalar field. The remaining error in PLIF measurements was mainly caused by (1) The standard deviation of the background images B, and (2) The uncertainty of κ $C_{dye,I}$ due to imperfect linearity. The effect of the standard deviation of the background images is evaluated by the signal-to-noise ratio (SNR). Due to the non-uniform illumination and the inhomogeneous dye concentration in the mixing region, the SNR varies among images and regions of the images. In our PLIF images recorded with a 12 bit CCD camera, the SNR was always greater than 50, resulting in an uncertainty less than 2% in the measurement of background gray level in Eq. (2). The uncertainty of $\kappa C_{dye,I}$ was found to be about 12% based on its mean and standard deviation. This uncertainty affects the measurement through the exponential term in Eq. (2), and the magnitude of this term was monitored during image processing and found to be greater than 0.65 but less than 1.0. Hence the ultimate uncertainty in the jet concentration ξ was less than 5.9%.

4 Results

Since the tee mixer's behavior is drastically different under various operational conditions, it is important to identify the scenarios. When a side jet is issued into the fully developed turbulent pipe flow, three scenarios can happen. Sroka and Forney (1989) used the parameter rd/D to characterize these scenarios.

- (1) **Jet-impaction regime** (rd/D>1.0): The jet hits the opposite wall of the pipe. Such impingement helps to break down large vortical structures and creates more efficient micromixing (Tosun, 1987). However, the impingement exerts significant stress on the pipe wall and thus such tee mixer designs are not desirable from the practical point of view.
- (2) **Jet-mixing regime** (0.07 < rd/D < 1): The jet penetrates into the potential core of the pipe flow, turns and aligns with the pipe flow. The jet expands quickly in the pipe due to turbulent entrainment and thus creates efficient macro mixing (Cozewith and Busko, 1989).
- (3) Wall-source regime (rd/D<0.07): The jet does not penetrate significantly into the pipe flow. It attaches to the pipe wall and grows slowly. Obviously, this scenario does not create efficient mixing and thus is not a desired operating condition.

In what follows we will concentrate on the jet-mixing regime and accordingly present PIV and PLIF measurement results for the tee mixer of r=3.06 unless otherwise specified. Only some of

the results for r=5.04 will be given. Following the convention in the literature on jet in crossflow, we will present these measurement results in figures with the jet shown as entering from the bottom, that is, upside down from Figure 1.

4.1 PIV measurements

From the PIV measurements of instantaneous velocity fields, one can gain insights into the flow physics of a jet in a confined crossflow and hence gain better understanding of the mixing mechanism and ways to improve designs. Furthermore, by averaging instantaneous realizations in each view various turbulence statistical quantities can be approximated. These statistical quantities are useful for CFD validation as well as mixing performance evaluation.

Figure 2(a) shows a typical instantaneous velocity field in the near field of the tee mixer measured on the center x-y plane from the side view by PIV. The corresponding spanwise vorticity field is shown in Figure 2(b). The high-speed jet fluid is identified in Figure 2(a), as well as the upward motion of the fluid behind the jet in the region where 1.5 < x/d < 3. The strong shear layer of the jet with spanwise roll-up resulting from instability is visualized in the vorticity contour plot. Figure 3 shows the side-view distribution of partial turbulent kinetic energy K calculated by $0.5\langle u^2\rangle + 0.5\langle v^2\rangle$. The region with large K values indicates strong turbulent mixing, which is a result of the interaction between the jet fluid and the upstream pipe fluid. Figure 4 shows the Reynolds shear stress $\langle u'w'\rangle$ in the top-view, where the jet enters the plane from the bottom and the pipe flow moves from left to the right. Two elongated, outward-tilted regions with concentrated high Reynolds stress are clearly seen in the figure.

4.2 PLIF measurements

The processing of the PLIF images provides instantaneous 2D pictures of the jet fluid concentration distribution. Time-resolved instantaneous recording of these pictures allows us to observe the mixing effect in a dynamical sense, while averaging 500 instantaneous pictures in each view provides the statistics of the concentration distribution. Based on these statistics we can cross check with the measured velocity fields the effects of flow structures on mixing, extract the jet characteristics, and compute the scalar PDF.

Figure 5 shows examples of the side-view instantaneous concentration (mixture fraction) field represented by 256 gray levels for both the r=3.06 and r=5.04 cases. The jet impingement for r=5.04 is evident from picture (b). In both pictures the penetration of the pipe fluid into the jet from the upstream side is observed. Spanwise roll-up of the jet shear layer is clearly visualized. It

is also noticed that the scale of these vortices is comparable to the size of the jet exit, which is the initial length scale of the scalar field.

Figure 6 displays the contours of mean concentration $\langle \xi \rangle$ of the side view calculated from the PLIF data for both r=3.06 and r=5.04 cases. The effect of jet impingement on the opposite pie wall is evident in (b). In both cases the mixed fluid expands more towards the downstream side of the jet, which indicates better mixing than on the upstream side of the jet.

Shown in Figure 7 are the contours of the variance of concentration $\langle \xi^2 \rangle$ of the side view and top view for r=3.06. In Figure 7(a), two regions are of particular interest: one is the region with the largest scalar variance on the upper half of the jet, which matches the region with the strong jet shear layer; the other is the branch of scalar variance that extends downstream behind the jet, which is related to vortex breakdown to be discussed below. In Figure 7(b), the region with the largest scalar variance is right on the upstream side of the jet entry in the top-view imaging plane.

5 Discussions

5.1 Flow structures

From our results it is observed that in absence of jet impingement the tee mixer bears some similarity to the jet in unconfined crossflow. Based on flow visualization, Fric and Roshko (1994) proposed a conceptual model of the jet in crossflow and identified four vortical structures: the jet shear layer with Kelvin-Helmholz vortices, the counter-rotating vortex pair (CVP) evolved from the jet after the jet has become aligned with the crossflow, the wake structures behind the jet column, and the horseshoe vortices just upstream of the jet exit. This model is sketched in Figure 8. Yuan et al. (1999) performed large eddy simulations (LES) of a jet in a crossflow. Their results not only confirmed the existence of all four vortical structures identified by Fric and Roshko (1994), but also revealed another vortical structure called hanging vortex. In what follows we examine the PIV and PLIF results obtained in the tee mixer (r=3.06) in the light of these vortical structures.

(1) **Jet Shear Layer:** In the vorticity contour shown in Figure 2(b), we can clearly visualize a strong shear layer on the *upper* half of the jet and the spanwise roll-up of this shear layer, which can also be identified from the PLIF snapshots shown in Figure 5(a). These rolled up vortices are responsible for entraining the pipe fluid into the jet. The jet shear layer is also visible from the variance of concentration shown in Figure 7(a), which indicates a correlation between energetic vortical structures and large scalar variance.

(2) Counter-rotating Vortex Pair (CVP): The best view of the streamwise CVP would be provided through the velocity and vorticity fields on the cross-sectional planes of the pipe (end view), but due to the restricted optical access of the tee mixer flow facility, this view could not be obtained. Nonetheless, the imprints of the CVP on statistical quantities can be found in the Reynolds stress and the concentration variance distributions from the top view, as shown in Figure 4 and Figure 7(b). These statistical quantities show the effect of mixing of the CVP.

Of the two legs with concentrated high Reynolds stress shown in Figure 4, the upper one has positive $\langle u'w' \rangle$ values, indicating correlated fluctuations along Quadrants I and III, while the lower one has negative $\langle u'w' \rangle$ values, indicating correlated fluctuations along Quadrants II and IV. These spatially distinguished, strongly correlated fluctuations suggest imprints of the vortex structures (CVP), whose rotation orientations are consistent with the Reynolds stress orientations. Hence, the CVP is outward tilted. This notion agrees with the general belief that the CVP is responsible for the jet expansion after the jet is aligned with the crossflow (Smith and Mungal, 1998). It is further noted that the elongated regions of high Reynolds stress $\langle u'w' \rangle$ start somewhere between $x/d = 3 \sim 4$. As seen in Figure 6(a), this is where the jet begins to be aligned with the pipe flow (and hence the start of the CVP). The CVP also leaves an imprint on the scalar field, as evidenced by the two branches in the concentration variance in the horizontal center plane shown in Figure 7(b). It should be pointed out that the structures exhibited in the Reynolds stress distribution do not directly reflect the vortex dynamics of the CVP. They only show the averaging effect of the instantaneous flow dynamics.

(3) Hanging Vortices: One of the prominent features noticeable in the time-series PLIF images (movie) of the tee mixer is that a stream of *mixed* fluid is seen continuously issued from the downstream side of the jet exit. This stream follows a short, nearly horizontal trajectory below the jet body and then moves up and joins the mixed fluid on the downstream side of the jet. This is illustrated with the white arrow drawn in Figure 5(a). The upward motion is also visible in the instantaneous velocity field (Figure 2(a)) at $x/d = 1.5 \sim 3$, which are outside the jet orifice. These are the same locations where the aforementioned stream becomes indiscernible from the neighboring fluid in the PLIF images. It is reasonable to postulate that this stream of mixed fluid is associated with the axial flow in the "hanging vortices" described by Yuan et al. (1999). The hanging vortices, originating from the instability of the skewed mixing layer between the jet and the crossflow on each lateral edge of the jet, produce important consequences for the downstream behavior of the jet. The strong axial flow in these vortices transports a significant amount of

scalar concentration, vorticity, and vertical momentum away from the jet body. Shortly downstream, these vortices break down into small vortices and generate upward motion.

The hanging vortices are important to the mixing because of their relationship with the CVP. Kelso et al. (1996) postulated that the circulation of CVP could be traced back to the tube-like structures that extend around the jet body and then up along the backside of the jet. Yuan et al. (1999) confirmed that these tube-like structures are the hanging vortices and suggested that the hanging vortices give rise to the CVP.

5.2 Jet characteristics in the tee mixer

The flow in a tee mixer has four basic geometric/flow parameters: the jet diameter d, the pipe diameter D, the jet-to-pipe velocity ratio r, and the pipe flow Reynolds number Re. The combination of rd, known as the jet momentum length, has been used as the parametric length scale for this flow (Sroka and Forney, 1989, Forney et al., 1996). Based on the momentum flux, the physical meaning of rd can be interpreted as the expanded diameter of the jet fluid after the jet is aligned with the pipe flow. As seen in the mean concentration contour in Figure 6(a), the width of the jet body (defined by ξ =0.1) is about rd when the jet bends over in the pipe.

(1) **Jet trajectories**: In the context of scalar mixing, we use the loci of the local maximum mean concentration to define the jet trajectory. Figure 9 shows the jet trajectories based on jet fluid concentration for two velocity ratios. The overlapping of two trajectories in the normalized coordinate suggests that the jet trajectory can be formulated by

$$\frac{y}{rd} \sim \left(\frac{x}{rd}\right)^n \tag{3}$$

Based on our PLIF data, we found n=0.4. Forney et al. (1999) studied the jet trajectories using a numerical procedure and found n=0.5. Maruyama et al. (1982) derived an empirical formula of jet trajectories and their near-field formula has n=0.46. It should be pointed out that no attempt was made to obtain the full expression of jet trajectory because only two velocity ratios and one jet injection angle were tested in this study.

(2) **Jet centerline decay**: The decay of the mean concentration $\langle \xi \rangle$ along the jet centerline is of great interest from the engineering point of view. The rate of the centerline decay provides a simple evaluation and a concise description of the scalar mixing. Based on the jet centerline consisting of the points with locally maximal mean concentration $\langle \xi \rangle$, we studied the decay of

 $\langle \xi \rangle$ by fitting the data along the jet centerline into an exponential form and defining the power of the exponential term as the decay rate.

For the mixing in the near field of tee mixer, the scalar (jet fluid concentration) decay along the jet centerline can be written as (Forney and Lee, 1982)

$$\langle \xi \rangle \sim r^a (\frac{x}{rd})^b$$
, (4)

where x can be taken as either the streamwise coordinate or the centerline marching distance, defined as the line integral along the jet centerline trajectory. The two parameters, a and b, are obtained by fitting the experimental data.

Figure 10 shows the decay versus the streamwise position x/rd for both r=3.06 and r=5.04. It is drawn on log-log scale so the power-law relationship appears as straight line. Clearly there is a transition of the decay rate for both cases. Before the transition the decay rate is -0.45, smaller than the decay rate of -2/3 after the transition. Since the transition occurs approximately at x=rd, the region after the transition is actually the region where the jet aligns with the pipe flow. For the jet decay in this region, Sroka and Forney (1989) have found the -2/3 decay rate using a similarity approach. The agreement between two results suggests that the similarity solution is valid for the tee-mixer flow in the region where x>rd.

(3) Jet expansion: When the jet goes downstream, it mixes with the crossflow and expands axially while its centerline concentration decreases. For the jet in an unconfined crossflow, no matter how far downstream it is observed there is always a boundary between the mixed fluid and the unmixed crossflow. In other words, both the jet and the crossflow are always well defined. However, when the jet expands in a confined crossflow (the tee mixer) the pipe will eventually be filled with the mixed fluid. After this happens neither the jet nor the crossflow can be distinguished and the flow becomes a turbulent pipe flow again. Clearly, the jet expansion and merging with the pipe flow is important in a tee mixer.

To examine the jet expansion we define the jet body using the 10% loci ($L_{10\%}$), which represent the points at which 10% of the jet fluid concentration is measured. The 10% level is chosen here because it is about the ultimate jet fluid concentration when the flow is fully mixed for the case of r=3.06. The expansion of the jet body is best examined from the end-view because the cross-sectional area occupied by the jet body would indicate the extent of the expansion. Although we did not conduct the end-view measurement due to the limited optical accessibility of the flow facility, we can approximately reconstruct the end-view using the side-view and top-view data. Since these data were taken at perpendicular center planes of the pipe, four $L_{10\%}$ points

can be transposed on to the end view. Figure 11 shows the jet expansion in reference to the tee mixer cross section area of the reconstructed jet. As the cross sectional area of the reconstructed jet increases from about 15% at x=0.5rd to 25% at x=1.8rd, the jet centerline mixture fraction decreases from 50% to 25%. It can be observed that after x=0.5rd, the jet expansion mainly occurs in the spanwise direction, while the jet is lifted in the wall-normal direction. This could be attributed to the counter-rotating vortex pair that exists in the jet in crossflow. It introduces common-up motion on the inner side and its outward tilting results in spreading in the spanwise direction.

(4) **Jet impingement**: There is no obvious criterion for determining if and when the jet body *starts* to impinge on the pipe wall. However, by identifying jet impingement as the intersection of the jet centerline with the opposite wall, we can use the jet trajectory to decide whether or not impingement of the jet is likely to happen for a given tee mixer design. It must be noted that the interaction between the jet and the wall starts actually before such "impingement" takes place.

If the jet becomes aligned with the pipe flow before it hits the wall, its centerline trajectory must satisfy the condition $y(x=x_a) < D$, where x_a is the streamwise position at which the jet is aligned with the pipe flow. Using the jet trajectory formula given by Eq. (3), it is straightforward to get the maximum rd that prohibits the occurrence of the jet impingement at the given pipe diameter:

$$(rd)_{\max} = D \cdot \left(\frac{\tan \beta}{n}\right)^{\frac{n}{1-n}},\tag{5}$$

where β is the angle between the jet centerline and the pipe centerline, n is the parameter in Eq. (3). With D/d = 6 and n=0.4, we get $r_{max} = 4.57$ when $\beta = 15^{\circ}$. Clearly, this is consistent with the experimental observation that the jet for r=3.06 was non-impinging and for r=5.04 was impinging. Here the value of β was chosen rather arbitrarily as an example. More in-depth research is required to provide a more reliable determination of β .

5.3 Scalar PDF across the jet shear layer

From a large quantity of measured concentration data, we can obtain the concentration probability density function distribution with respect to the location in the near field of the tee mixer. Like in the case of simple shear layer mixing, the behavior of the scalar PDF across the jet in the tee mixer can shed light on the mixing mechanism.

In shear layer mixing the variation of the scalar PDF across the mixing layer reveals the dominant mechanism for mixing. Three idealized cases of the variation were given by Karasso and Mungal (1996) and shown in Figure 12. If large-scale structures dominate and the mixing is mainly through entrainment by vortices instead of gradient transport, the most probable value of concentration is invariant across the mixing region [Figure 12(a)]. In this case, large-scale structures induce *homogeneous* mixing across the layer at a composition ratio equal to the entrainment ratio. On the other hand, if enough small eddies are produced, the turbulent diffusion becomes important and a potential scalar gradient along the mixing layer is generated by this diffusion. Therefore the most probable value of concentration marches across the layer and takes the average concentration at that transverse location [Figure 12(b)]. Intermediate to the non-marching type [Figure 12(a)] and marching type [Figure 12(b)] is the tilted PDF, which slants toward the average concentration [Figure 12(c)].

In the near field of the tee mixer the mixing layer is formed around the jet column. On the jet center plane in the side view two mixing layers are present: one above and the other below the jet centerline. The scalar PDF across the jet column region can therefore be viewed as the scalar PDF across two adjacent shear layers. To examine the variation of the PDF in these two mixing layers we use the PDF of the concentration at points on lines perpendicular to the jet centerline as illustrated in Figure 13. To compute the concentration PDF at a given point *x*

$$pdf(\xi, x) \cdot \Delta \xi = probability\{\xi - \frac{\Delta \xi}{2} < \xi(x) < \xi + \frac{\Delta \xi}{2}\},$$
 (6)

we choose $\Delta \xi$ to be 2% based on the number of realizations and the magnitude of measurement uncertainty.

Figure 14 shows the contour of the measured concentration PDF across the jet at x=2.0rd. Since the jet is already aligned with the pipe at this streamwise location, the line perpendicular to the jet is the y-axis. The whole jet column defined by $\langle \xi \rangle > 10\%$ covers the range of y from 0.15D to 0.75D, and the position of the jet centerline at this streamwise position is at y=0.56D. The scalar PDF across the upper mixing layer $(y=0.75D\ to\ 0.56D)$ is easily identified as the non-marching PDF because the upper half of the contour in Figure 14 does not shift with respect to ξ , whereas the scalar PDF across the lower mixing layer could be seen as a combination of the tilted PDF and the marching PDF. The concentration PDF variation across the jet is also checked using the measured PDF at sampling points along the line perpendicular to the jet centerline at x=1.0rd, as plotted in Figure 15. The positions of these points are sketched in Figure 13. A non-marching PDF is evident in the upper mixing layer (points a, b, c, and d) where the peaks of PDF do not shift significantly, whereas a marching PDF is clearly seen in the lower mixing layer (points e, f, g, and h) with the peaks shifting towards $\xi=0$.

These results prove that the turbulent mixing on the upstream side of the jet (above the jet centerline) is mainly performed by large-scale structures, and on the downstream side by turbulent diffusion. Therefore, when it is applied in a CFD simulation of the mixing in the near field of tee mixer, the eddy viscosity model is more likely to fail on the upstream side of the jet than on the downstream side.

5.4 Validity of the presumed β -PDF

The presumed PDF method is commonly used in the CFD approach for fast chemical reactions because the chemical reaction term can be closed by the scalar PDF if equilibrium in each fluid particle is reached. One of the widely used presumed PDF in binary mixing is the presumed β -PDF, which is constructed using the first and second moments of the scalar value. Previous works on the validation of the presumed β -PDF in turbulent mixing flow have been reported by Madnia et al. (1991) and Frankel et al. (1992). They compared the presumed β -PDF with the scalar PDF constructed from their direct numerical simulation (DNS) data in both homogenous turbulent flow and turbulent shear flow and found that the presumed β -PDF is a good approximation of the scalar PDF.

To validate the presumed β -PDF in the tee mixer flow, we compared the presumed β -PDF with the experimental data at points across the bending jet in the pipe. The presumed β -PDF $f(\xi)$ is computed using the experimental scalar mean and variance data according to the formula given below,

$$f(\xi) = \frac{\xi^{\alpha - 1} (1 - \xi)^{\beta - 1}}{\int_{-1}^{1} \xi^{\alpha - 1} (1 - \xi)^{\beta - 1}},$$
(7)

where
$$\alpha = \langle \xi \rangle \left[\frac{\langle \xi \rangle (1 - \langle \xi \rangle)}{\langle \xi^{2} \rangle} - 1 \right]$$
, $\beta = \alpha \cdot \frac{1 - \langle \xi \rangle}{\langle \xi \rangle}$, $\langle \xi \rangle$ and $\langle \xi^{2} \rangle$ are the mean and variance

of concentration ξ , respectively*.

Figure 16 shows the comparison between the β -PDF and the measured scalar PDF at the eight points at position x = 2.0rd, where the smooth curves are the β -PDF data and the step-wise curves are the experimental data. It is seen that in the lower mixing layer (points e, f, g, h) the β -PDF not

16

^{*} FLUENT User's Guide Vol. 2, 1998

only captures the shape and the range of the measured PDF, but also matches the values reasonably well. However, in the upper mixing layer (points a, b, c, d) there is a significant discrepancy between the β -PDF and the measured scalar PDF. The difference in the performance of the β -PDF is due to the distinction between the dominant mixing mechanisms in the different regions of the tee mixer. When the dominant mechanism of the mixing is the turbulent diffusion, better performance of the β -PDF is achieved. If the mixing is mainly contributed by large-scale structures, the β -PDF is at most a rough approximation for the scalar PDF.

6 Conclusions

Particle Image Velocimetry (PIV) and Planar Laser Induced Fluorescence (PLIF) have been used to provide two-dimensional velocity and concentration field data for studying turbulent scalar mixing in the near field of a tee mixer (transverse jet in a pipe). The experimental techniques described here include a PLIF setup using sodium fluorescein and Nd:YAG laser and a quasi-ratiometric method to remove the influence of illumination inhomogeneity in the PLIF measurement. Typical flow structures in the tee mixer are revealed by instantaneous PIV and PLIF measurement data, and their roles in scalar mixing are discussed. Turbulence statistics including turbulence kinetic energy and Reynolds shear stresses are calculated from two-dimensional velocity field data, and scalar statistics including mean, variance, and probability density function (PDF) are calculated from the two-dimensional concentration field data. These data can be used to validate CFD simulations for tee mixers. The following observations are made from direct analysis of our measurement data:

- (1) Under moderate jet-to-pipe velocity ratios at which the jet merges with the pipe core, the tee mixer in the near field behaves similar to the jet in unconfined crossflow.
- (2) In a tee mixer the jet centerline concentration decays as $x^{-2/3}$ after the jet aligns with the pipe flow. This agrees with the theoretical result obtained by Sroka and Forney (1989). In the region where the jet is bending, the jet centerline concentration decays as $x^{-0.45}$.
- (3) In the near field of the tee mixer, the mixing in the upper mixing layer of the jet is dominated by the large-scale vortex structures, whereas in the lower mixing layer it is mainly accomplished by small eddies and turbulent diffusion. This difference is illustrated in the non-marching PDF across the shear layer on the upstream side of the jet and marching PDF on the downstream side.
- (4) The presumed β -PDF is an excellent approximation of the scalar PDF in the regions where the mixing is mainly done by small-scale structures (such as the downstream side of the issuing transverse jet). However, in the regions dominated by large-scale structures (such as the upstream

side of the issuing transverse jet) the β -PDF does not compare very well with experimental results.

Finally it must be pointed out that although cross-referencing of the velocity fields and scalar fields at the statistical level provides some insights into the mixing mechanism, detailed correlations between velocity and scalar (as needed to compute the scalar flux) would require simultaneous velocity and scalar measurements. This calls for the development of simultaneous PIV/PLIF techniques (Frank et al., 1996, Rehm and Clemens, 1998, Carter et al., 1998).

7 Acknowledgement

This work was sponsored by the Dow Chemical Company through a matching grant to an NSF CAREER award (CTS-9625306). The majority of the work was conducted when the authors were with Kansas State University. Guidance from Subrata Sen and Chuck Lipp from the Dow Chemical Company is greatly appreciated. The authors wish to thank Wenming Yang for the construction of the tee mixer experimental facility and assistance in the PIV data acquisition and processing. They also wish to thank Rodney O. Fox for helpful discussions.

8 Literature Cited

- Brodkey, R. S., The Phenomena of Fluid Motions, Addison Wesley Publishing Co. (1967).
- Carter, C. D., J. M. Donbar, and J. F. Driscoll, "Simultaneous CH Planar Laser-induced Fluorescence and Particle Imaging Velocimetry in Turbulent Non-premixed Flames", *Applied Physics B: Lasers and Optics*, **66**, 129 (1998).
- Catalano, G. D., J. A. Mathis, and K. S. Chang, "Higher-order Statistics of a Turbulent Jet in a Confined Crossflow", *AIAA Journal*, **29**(12), 2124 (1991).
- Cozewith, C and M. Busko, "Design Correlation for Mixing Tees," *Ind. and Eng. Chem. Res.*, **28**, 1521 (1989).
- Dahm, W. J. A., K. B. Southerland, and K. A. Buch, "Direct, High resolution, Four-dimensional Measurements of the Fine Scale Structure of Sc>>1 Molecular Mixing in Turbulent Flows," *Phys Fluids A*, **3**, 1115 (1991).
- Forney, L. J. and T. C. Kwon, "Efficient Single Jet Mixing in Turbulent Tube Flow," *AIChE J.*, **25**, 623 (1979).
- Forney, L. J. and H. C. Lee, "Optimum Dimensions for Pipeline Mixing at a T-Junction," *AIChE J.*, **28**, 980 (1982).
- Forney, L. J., N. Nafia, and H. X. Vo, "Optimum Jet Mixing in a Tubular Reactor," *AIChE J.*, **42**, 3113 (1996).

- Forney, L. J., Z. Feng, and X. Wang, "Jet Trajectories of Transverse Mixers at Arbitrary Angle in Turbulent Tube Flow" *Trans IChemE*, **77**, 754 (1999).
- Fric, T. F. and A. Roshko, "Vortical Structure in the Wake of a Transverse Jet," *J. Fluid Mech.*, **279**, 1 (1994).
- Frank, J. H., K. M. Lyons and M. B. Long, "Simultaneous Scalar/Velocity Field Measurements in Turbulent Gas-Phase Flows", *Combustion and Flame*, **107**, 1 (1996).
- Frankel, S. H., C. K. Madnia, and P. Givi, "Modeling of The Reactant Conversion Rate In a Turbulent Shear Flow," *Chem. Eng. Comm.*, **113**, 197 (1992).
- Gosman, A. D., R. Simitovic, "An Experimental Study of Confined Jet Mixing," *Chem. Eng. Sci.*, **41**, 1853 (1986).
- Hatch, M. S., W. A. Sowa, G. S. Samuelsen, J. D. Holdeman, "Geometry and Flow Influences on Jet mixing in a Cylindrical Duct", *J. Propulsion and Power*, **11**, 402 (1995).
- Karasso, P. S. and M. G. Mungal, "Scalar Mixing and Reaction in Plane Liquid Shear Layers," *J. Fluid Mech.*, **323**, 23 (1996).
- Karasso, P. S. and M. G. Mungal, "PLIF Measurements in Aqueous Flows Using Nd:YAG Laser," *Exp. in Fluids*, **23**, 382 (1997).
- Keane, R. D. and R. J. Adrian, "Theory of Cross-correlation Analysis of PIV Images", *App. Sci. Res.*, **49** 191 (1992).
- Kelso, R. M., T. T. Lim, and A. E. Perry, "An Experimental Study of Round Jets in Cross-flow," *J. Fluid Mech.*, **306**, 111 (1996).
- Koochesfahani, M. M. and P. E. Dimotakis, "Laser-Induced Fluorescence Measurements of Mixed Fluid Concentration in a Liquid Plane Shear Layer," *AIAA J.*, **23** (11), 1700 (1985).
- Madnia, C. K., S. H. Frankel, and P. Givi, "Direct Numerical Simulation of the Unmixedness in a Homogeneous Reacting Turbulent Flow," *Chem. Eng. Comm.*, **109**, 19 (1991).
- Maruyama, T., S. Suzuki, and T. Mizushina, "Pipeline Mixing Between Two Fluid Streams Meeting at a T-junction," *Int. Chem. Eng.*, **21**, 205 (1981).
- Maruyama, T., T. Mizushina and F. Watanabe, "Turbulent Mixing of Two Fluid Streams at an Oblique Branch," *Int. Chem. Eng.*, **22**, 287 (1982).
- Rehm, J. E. and N. T. Clemens, "Relationship Between Vorticity/Strain and Reaction Zone Structure in Turbulent Non-premixed Jet Flames", *Proceedings of the 27th International Symposium on Combustion*, **27**, 1173 (1998).
- Smith, S. H. and M. G. Mungal, "Mixing, Structure and Scaling of the Jet in Crossflow," *J. Fluid Mech.*, **357**, 83 (1998).

Sroka, L. M. and L. J. Forney, "Fluid Mixing with a Pipeline Tee: Theory and Experiment", *AIChE J.*, **35**, 406 (1989).

Tosun, G., "A Study of Micromixing in Tee Mixers," *Ind. and Eng. Chem. Res.*, **26**, 1184 (1987). Unger, D. R. and F. J. Muzino, "Laser-induced Fluorescence Technique for the Quantification of Mixing in Impinging Jets", *AIChE J.*, **45**, 2477 (1999).

Westerweel, J., "Fundamentals of Digital Particle Image Velocimetry", *Measurement Science & Technology*, **8**, 1379 (1997).

Yuan, L. L., R. L. Street, and J. H. Ferziger, "Large-eddy Simulations of a Round Jet in Crossflow," *J. Fluid Mech.*, **379**, 71 (1999).

Appendix: Linear response of sodium fluorescein with Nd:YAG laser

According to the Beer's law, a laser beam propagating through an absorbing medium decreases in intensity exponentially along the propagation:

$$I_{y} = I_{0} \cdot \exp(\int_{0}^{y} \kappa \cdot C_{dye} \cdot dy), \qquad (A1)$$

where I is the laser intensity, κ is the absorption coefficient, C_{dye} is the dye concentration, and y is the distance along the direction of laser propagation. For a uniformly diluted dye concentration and in the absence of saturation and bleaching effect, Beer's law implies that the logarithmic laser intensity should decrease linearly with distance of laser propagation. If the fluorescence emission response of the dye is linear with the laser intensity, then the logarithmic fluorescence signal should decrease linearly with distance in a dye cell at a uniformly diluted concentration.

Karasso and Mungal (1997) found that for the sodium-fluorescein/Nd:YAG laser combination the fluorescence response was nonlinear with distance. To verify their observation we performed calibration experiments using both a New Wave Nd:YAG laser (20mJ per pulse at 532nm) and a Spectra Physics PIV-400 Nd:YAG laser (400mJ per pulse at 532nm). In each experiment a uniformly collimated laser light sheet was passed through a rectangular sodium fluorescein cell at a uniform dye concentration of 0.1 mol/m³, and digital pictures of the fluorescent light sheet in the dye cell were recorded laterally to give the fluorescent intensity. In both experiments we observed a nonlinear behavior similar to what Karasso and Mungal described; the fluorescence intensity actually increased with distance before it decreased. This abnormal behavior could be attributed to many factors including optical trapping (absorption of emitted fluorescence). It implies nonlinear excitation: the fluorescence does not respond linearly with laser intensity. However, we

have noticed two characteristics of this "non-linearity" from both our data and those reported by Karasso and Mungal (1997): (a) The non-linear response, manifested as an increase of fluorescence intensity along the direction of laser propagation, exists only within a short distance from the laser entry point in the dye cell. After such a distance, the intensity decreases almost linearly in the propagation direction. (b) When the laser power is decreased, the peak fluorescence intensity (starting point of the linear region) shifts towards the laser entry point.

Based on these two observations, we designed a method to remove the non-linear region from the PLIF imaging window by adding a dye cell in the laser path just before the PLIF measurement region. This pre-entry dye cell, intended to contain the non-linear response segment, was a rectangular chamber with uniform dye solution placed immediately outside the testing tube. With the use of this cell, the dye in the test region achieves a linear response as shown by the In-situ calibration experiments. The linear regression of the results of $\ln(I_n/I_0)$ vs. y has a slope of about -0.046, and a correlation coefficient greater than 0.99. The error of concentration measurement caused by the deviation from linearity is less than 5.2%. This verifies the dye's linear response to the laser excitation within the test region in our experiment.

Figure Captions

- Figure 1. Tee mixer flow facility for the experiments
- Figure 2. Instantaneous two-dimensional velocity field (a) and spanwise vorticity field (b) on the center plane of the tee mixer (side view, covering the pipe diameter) measured by PIV. Dashed contours in (b) indicate negative values. The jet entry was at (0, 0), and the jet-to-pipe velocity ratio was 3.06.
- Figure 3. Partial turbulent kinetic energy ($0.5\langle u^{'2}\rangle + 0.5\langle v^{'2}\rangle$) on the side-view center plane.
- Figure 4. Reynolds stress $\langle u'w' \rangle$ on the top-view center plane. The jet entered the plane from the bottom and the pipe flow moved from the left side to the right side.
- Figure 5. Gray level images of the side-view instantaneous concentration field for both (a) r=3.06 and (b) r=5.04. The image domain covered the pipe diameter. The jet entered from the bottom and turns with the pipe flow. The white arrow indicates an observed stream of mixed fluid.
- Figure 6. Contours of mean concentration $\langle \xi \rangle$ on the center plane (side view, covering the pipe diameter) calculated from the PLIF data for (a) r=3.06, (b) r=5.04.
- Figure 7. Contours of variance of concentration $\left\langle \xi^{'2} \right\rangle$ for r=3.06 (a) on the side-view center plane, (b) on the top-view center plane.
- Figure 8. A conceptual model of the jet in (unconfined) crossflow given by Fric and Roshko (1994) including four vortical structures.
- Figure 9. Jet trajectories based on jet fluid concentration for r=3.06 (curve A) and r=5.04 (curve B): (a) coordinates normalized by d; (b) coordinates normalized by rd. The jet entry was at (0, 0).
- Figure 10. Decay of the mean jet fluid concentration along the jet centerline with respect to x for two velocity ratios (A: r=3.06, B: r=5.04).
- Figure 11. Jet expansion shown in reference to the tee mixer geometry for r=3.06. The shaded area represents the region with $\langle \xi \rangle$ > 10%, and the dashed line is the jet centerline.
- Figure 12. Three idealized types of scalar PDF across a shear layer given by Karasso & Mungal (1996): (a) non-marching PDF, (b) marching PDF, (c) tilted PDF.
- Figure 13. Sketch of the positions of the sampling points (denoted by $a \sim h$) at which the measured scalar PDF are plotted in Figures 14, 15, and 16. These points are along the lines perpendicular to the jet centerline.

- Figure 14. Contour of measured concentration PDF at x=2.0rd across the jet from y=0.15D to y=0.75D.
- Figure 15. Measured concentration PDF at the eight sampling points (positions shown in Figure 13) along the line perpendicular to the jet centerline at x=1.0rd.
- Figure 16. Measured concentration PDF (step-wise curve) and the calculated β -PDF (smooth curve) at the eight sampling points (positions shown in Figure 13) along the line perpendicular to the jet centerline at x=2.0rd.

Table

Table 1: Flow conditions

| | Jet flow ($d = 1.27$ cm) | | Pipe flow ($D = 7.62$ cm) | |
|------|---------------------------|--------|----------------------------|--------|
| r | U_j (cm/s) | Re_j | U_p (cm/s) | Re |
| 3.06 | 84.7 | 10,630 | 27.7 | 20,850 |
| 5.04 | 139.5 | 17,500 | 27.7 | 20,850 |

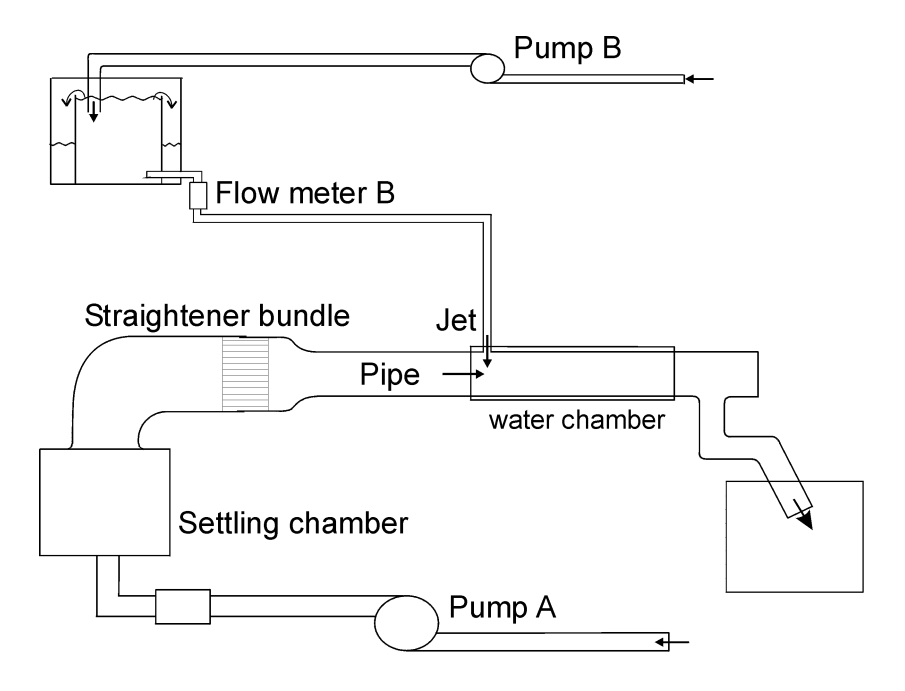


Figure 1. Tee mixer flow facility for the experiments

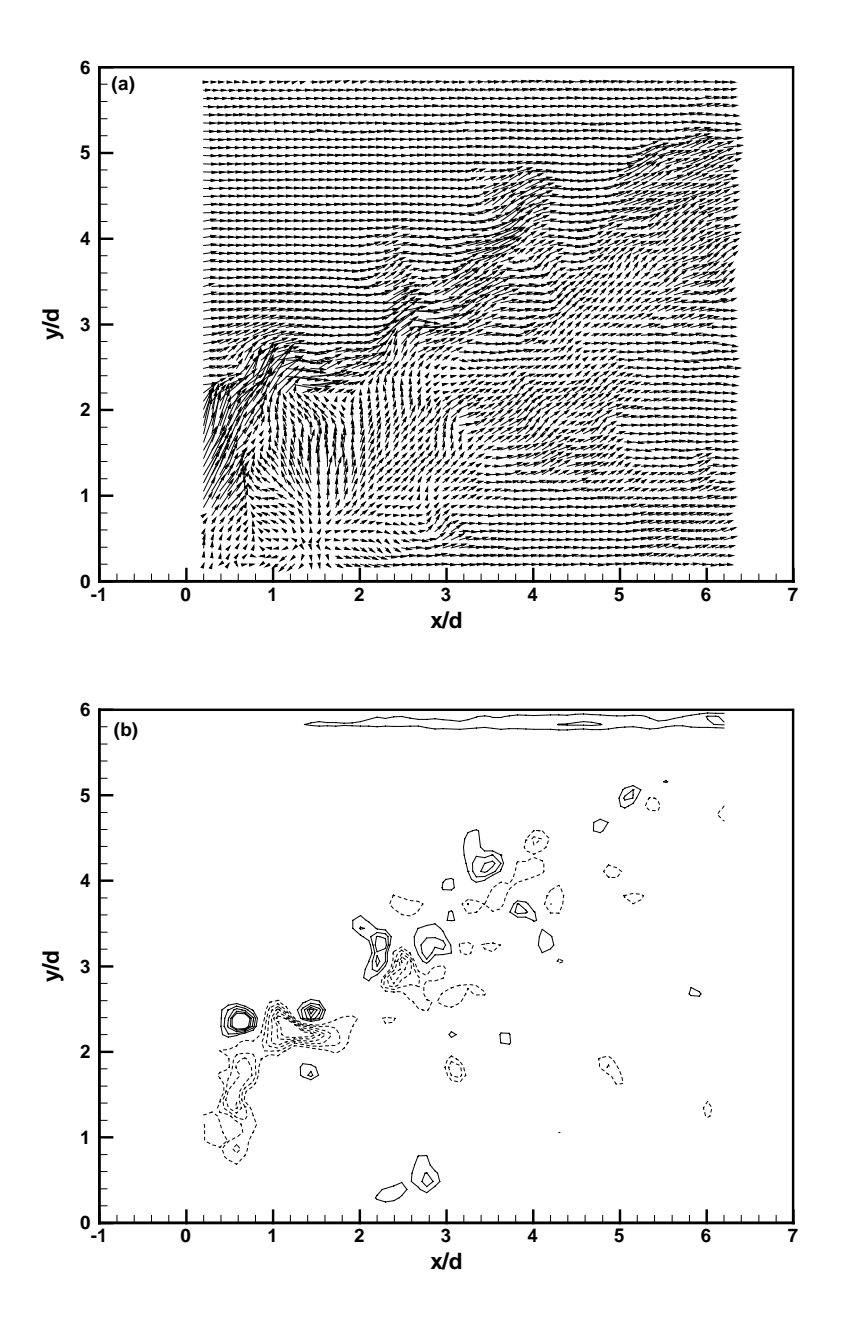


Figure 2. Instantaneous two-dimensional velocity field (a) and spanwise vorticity field (b) on the center plane of the tee mixer (side view, covering the pipe diameter) measured by PIV. Dashed contours in (b) indicate negative values. The jet entry was at (0, 0), and the jet-to-pipe velocity ratio was 3.06.

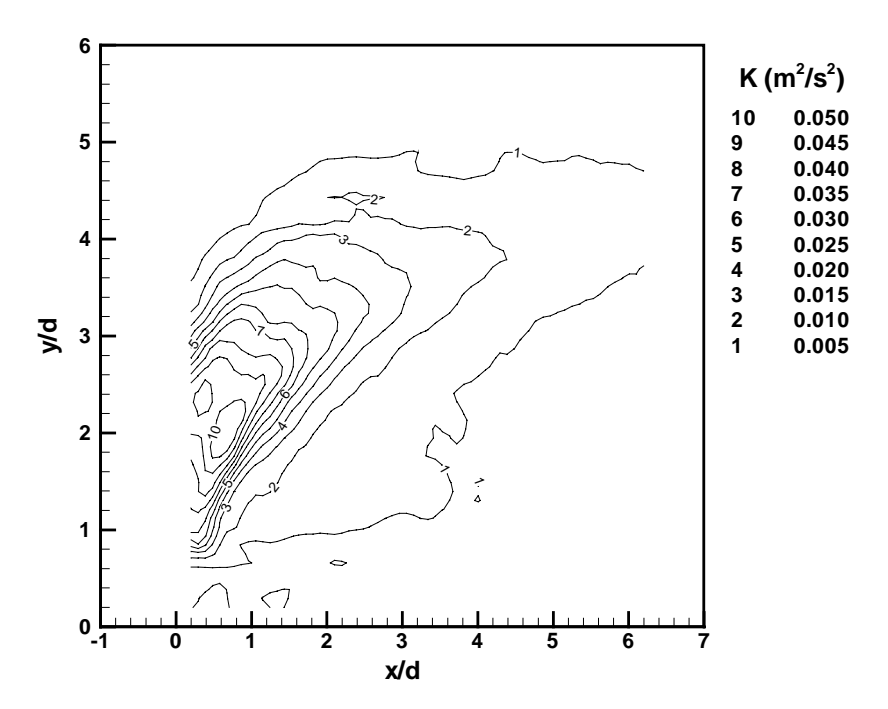


Figure 3. Partial turbulent kinetic energy ($0.5 \left< u^{'2} \right> + 0.5 \left< v^{'2} \right>$) on the side-view center plane.

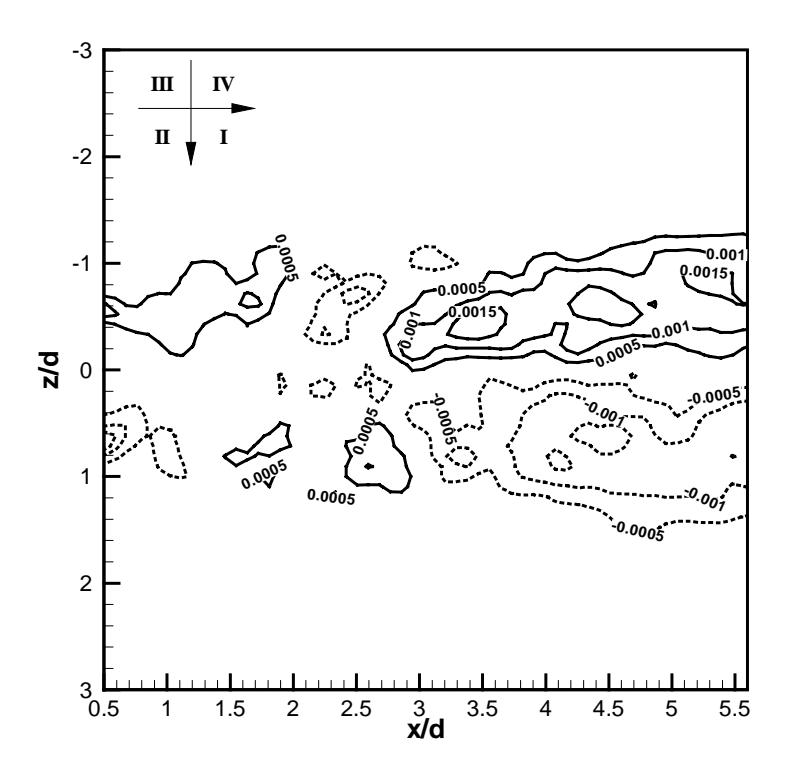


Figure 4. Reynolds stress $\langle u'w' \rangle$ on the top-view center plane. The jet entered the plane from the bottom and the pipe flow moved from the left side to the right side.

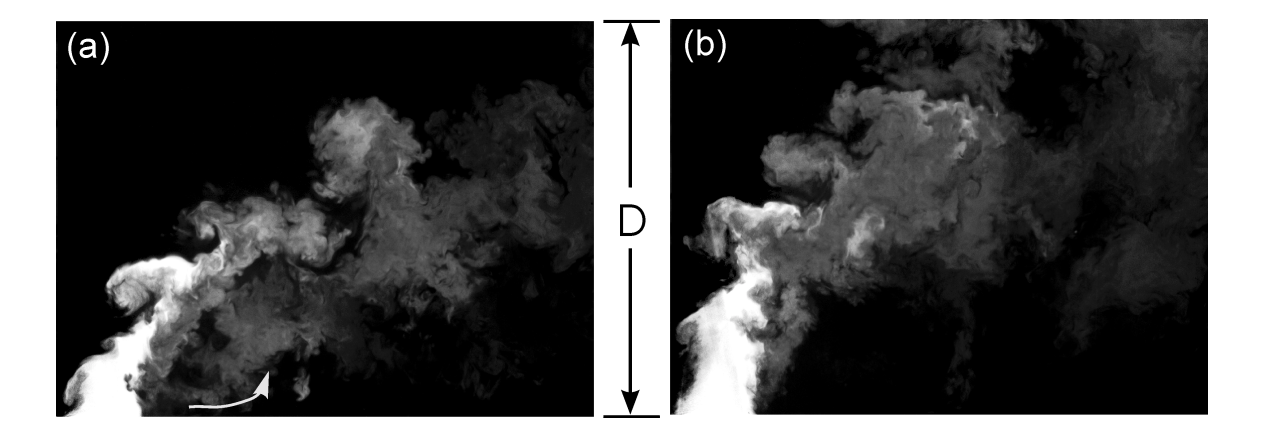


Figure 5. Gray level images of the side-view instantaneous concentration field for both (a) r=3.06 and (b) r=5.04. The image domain covered the pipe diameter. The jet entered from the bottom and turns with the pipe flow. The white arrow indicates an observed stream of mixed fluid.

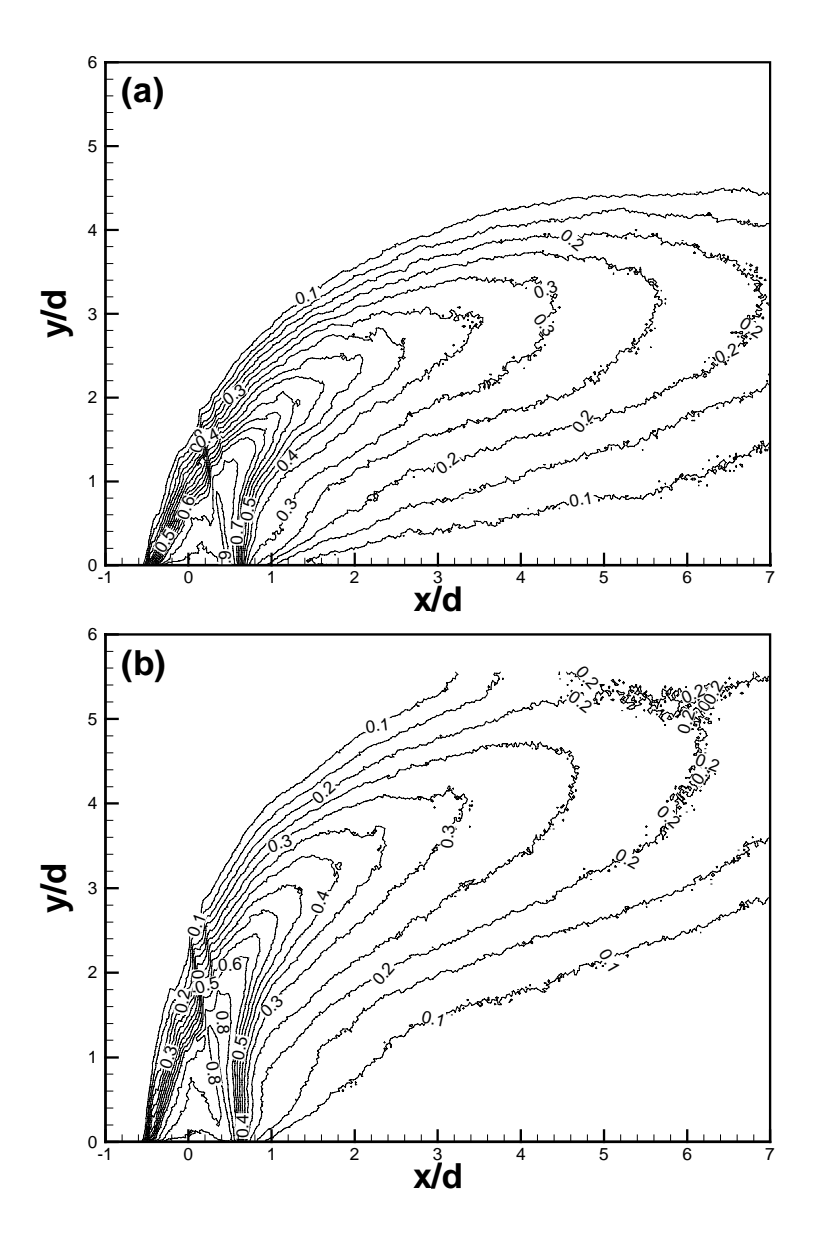


Figure 6. Contours of mean concentration $\langle \xi \rangle$ on the center plane (side view, covering the pipe diameter) calculated from the PLIF data for (a) r=3.06, (b) r=5.04.

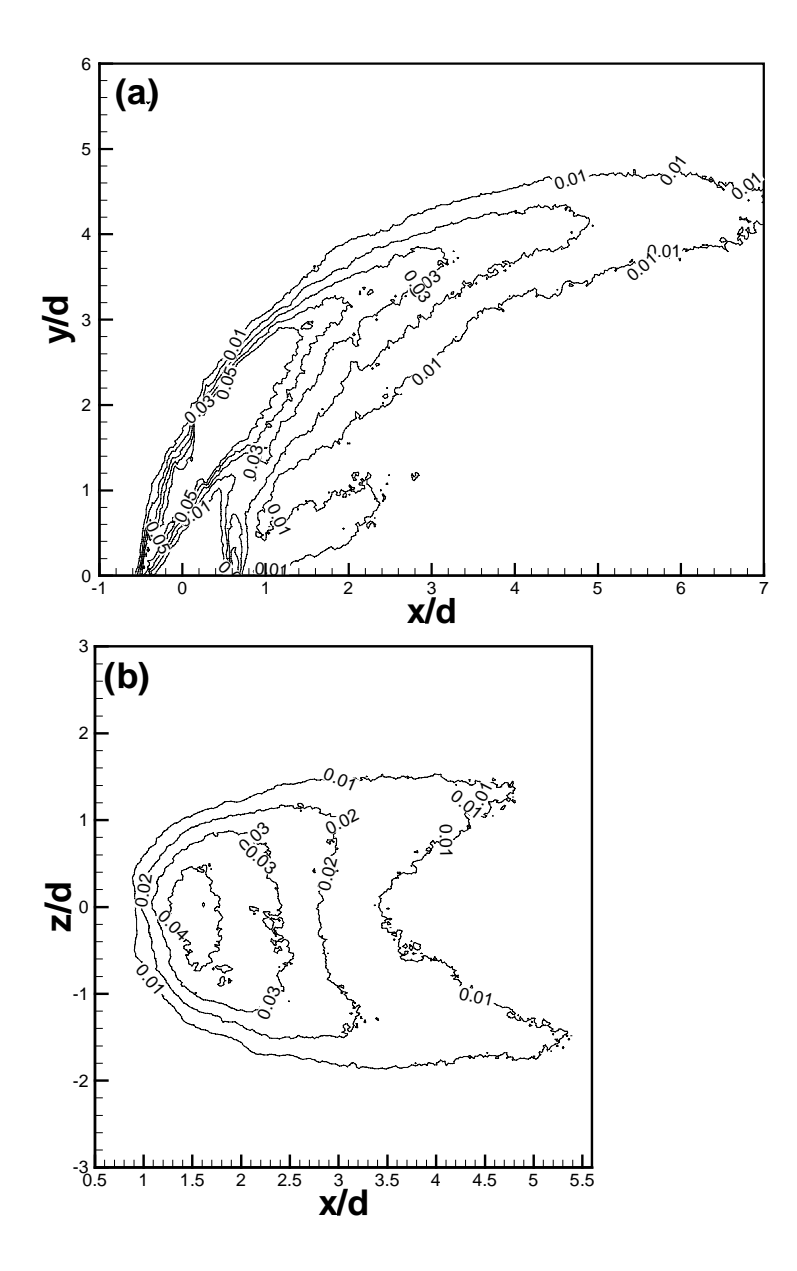


Figure 7. Contours of variance of concentration $\left<\xi^{'2}\right>$ for r=3.06 (a) on the side-view center plane, (b) on the top-view center plane.

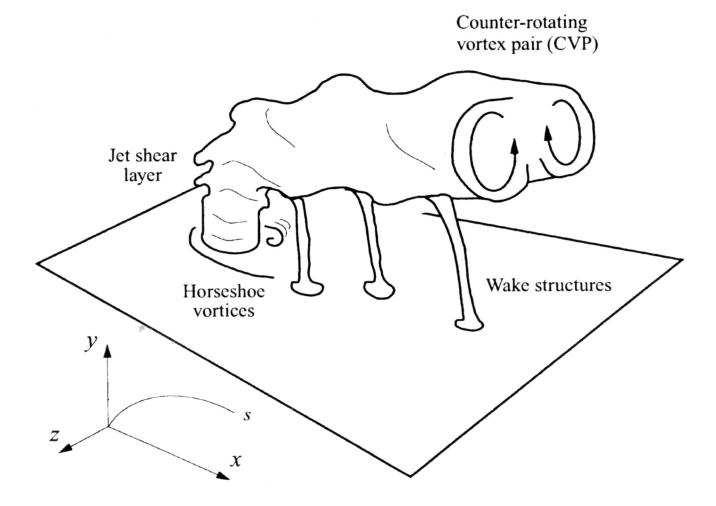


Figure 8. A conceptual model of the jet in (unconfined) crossflow given by Fric and Roshko (1994) including four vortical structures.

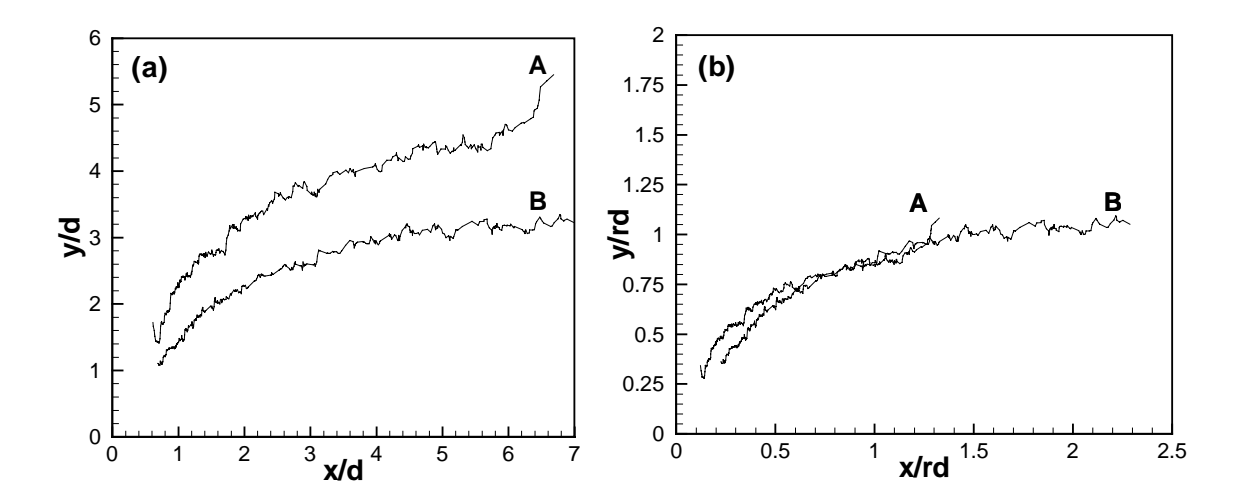


Figure 9. Jet centerline trajectories based on jet fluid concentration for r=3.06 (curve A) and r=5.04 (curve B): (a) coordinates normalized by d; (b) coordinates normalized by rd. The jet entry was at (0, 0).

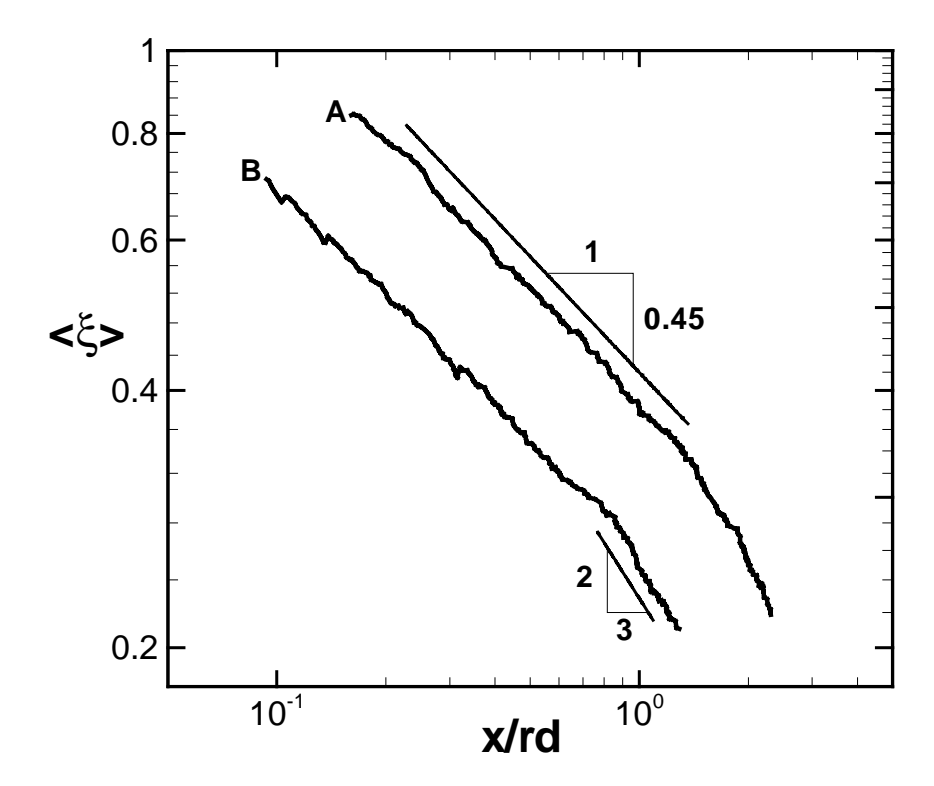


Figure 10. Decay of the mean jet fluid concentration along the jet centerline with respect to x for two velocity ratios (A: r=3.06, B: r=5.04).

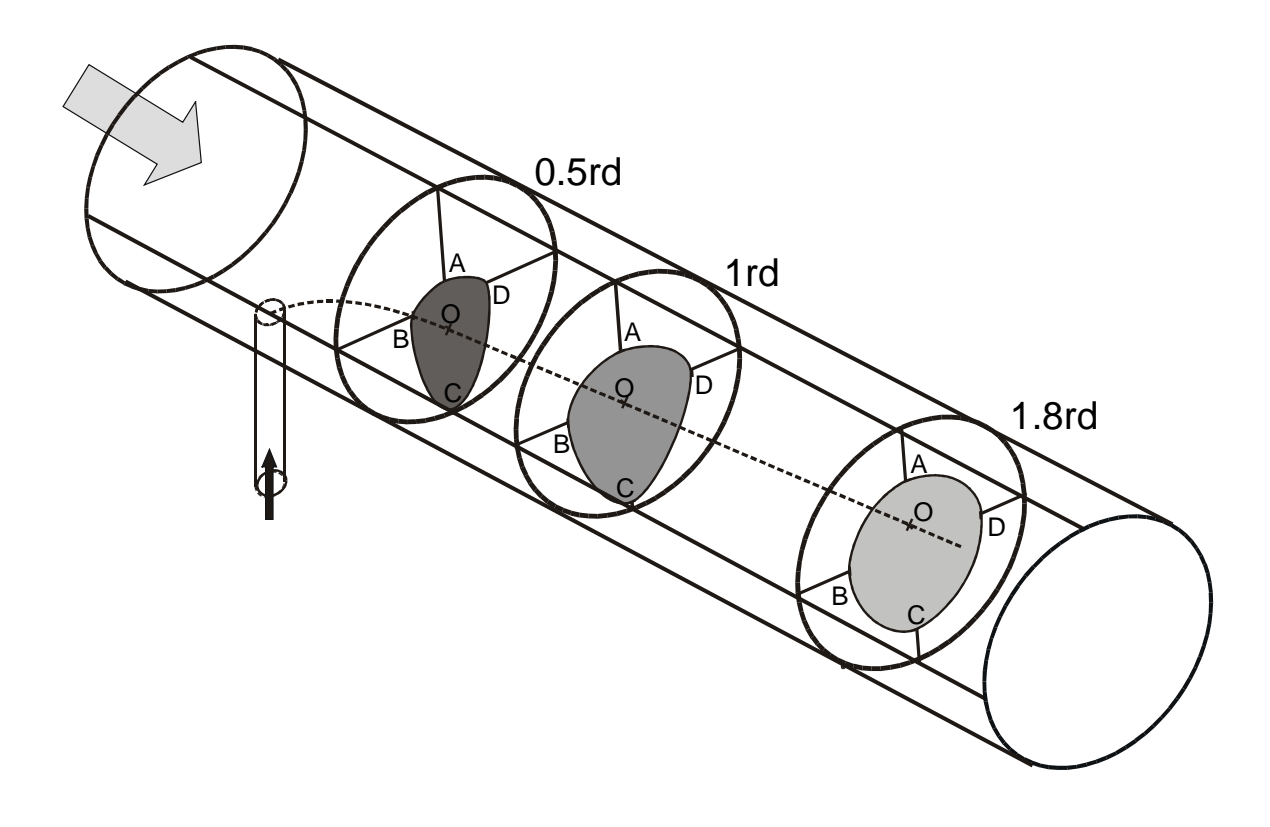


Figure 11. Jet expansion shown in reference to the tee mixer geometry for r=3.06. The filled area represents the region with $\langle \xi \rangle$ > 10%, and the dashed line is the jet centerline.

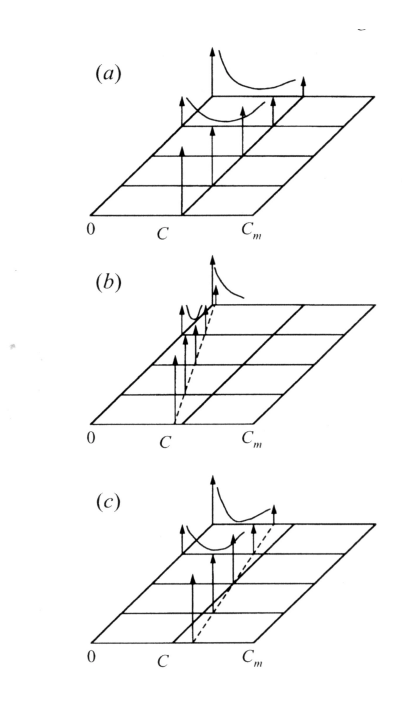


Figure 12. Three idealized types of scalar PDF across a shear layer given by Karasso & Mungal (1996): (a) non-marching PDF, (b) marching PDF, (c) tilted PDF.

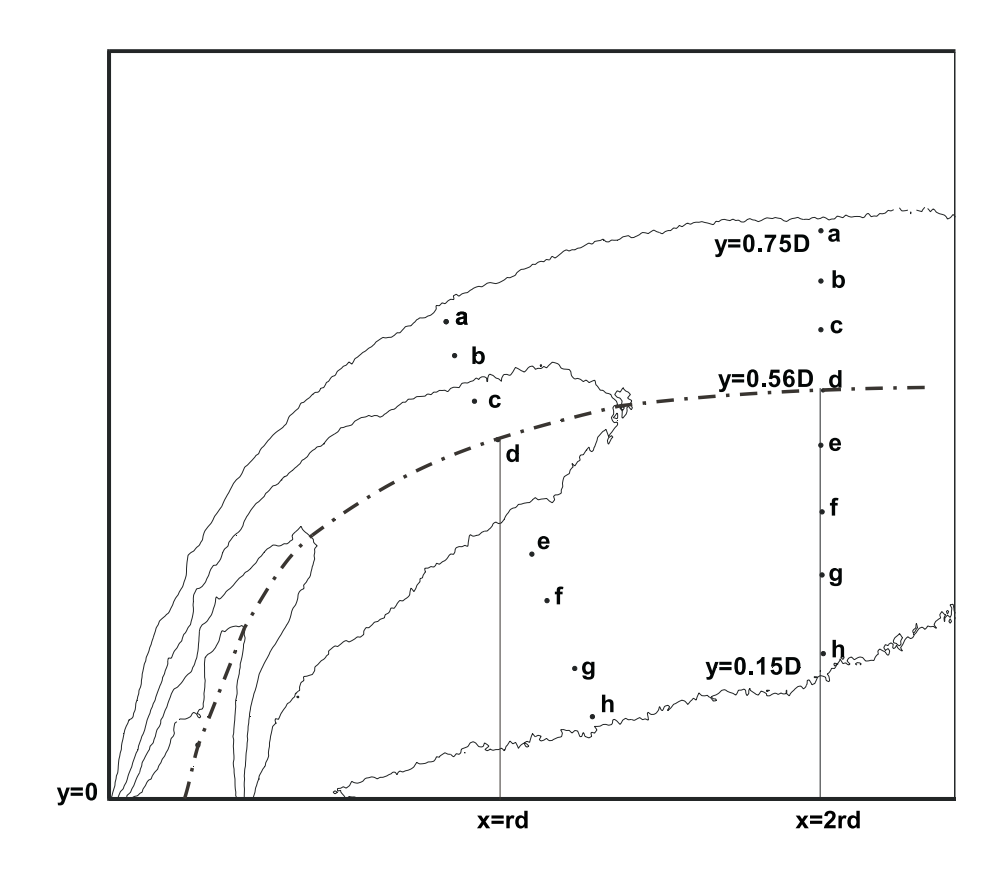


Figure 13. Sketch of the positions of the sampling points (denoted by $a \sim h$) at which the measured scalar PDF are plotted in Figures 14, 15, and 16. These points are along the lines perpendicular to the jet centerline.

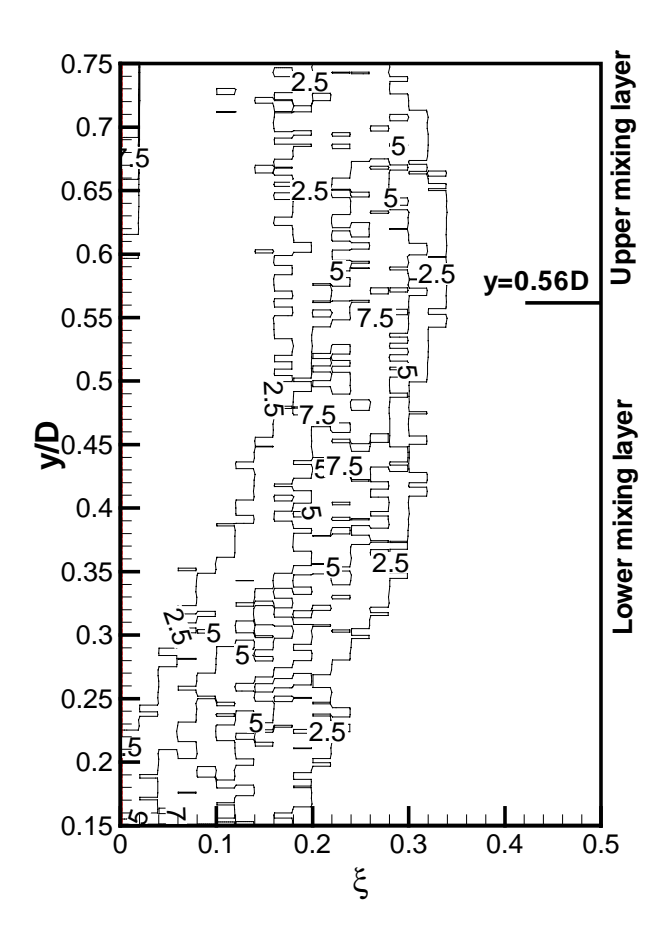


Figure 14. Contour of measured concentration PDF at x=2.0rd across the jet from y=0.15D to y=0.75D.

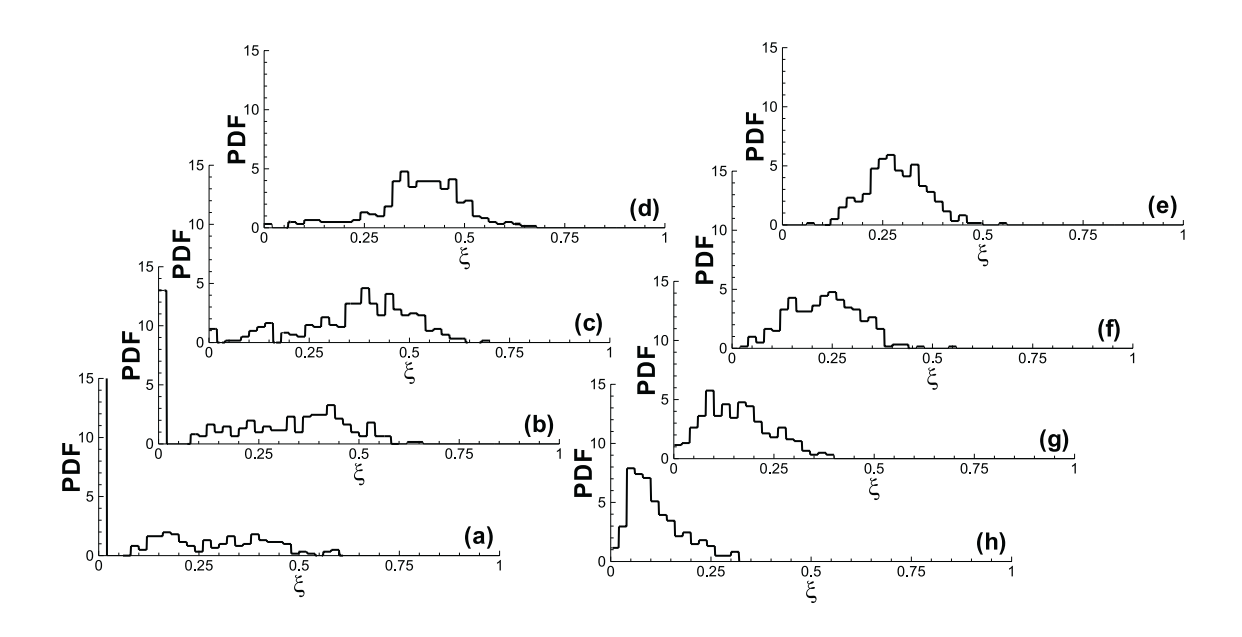


Figure 15. Measured concentration PDF at the eight sampling points (positions shown in Figure 13) along the line perpendicular to the jet centerline at x=1.0rd.

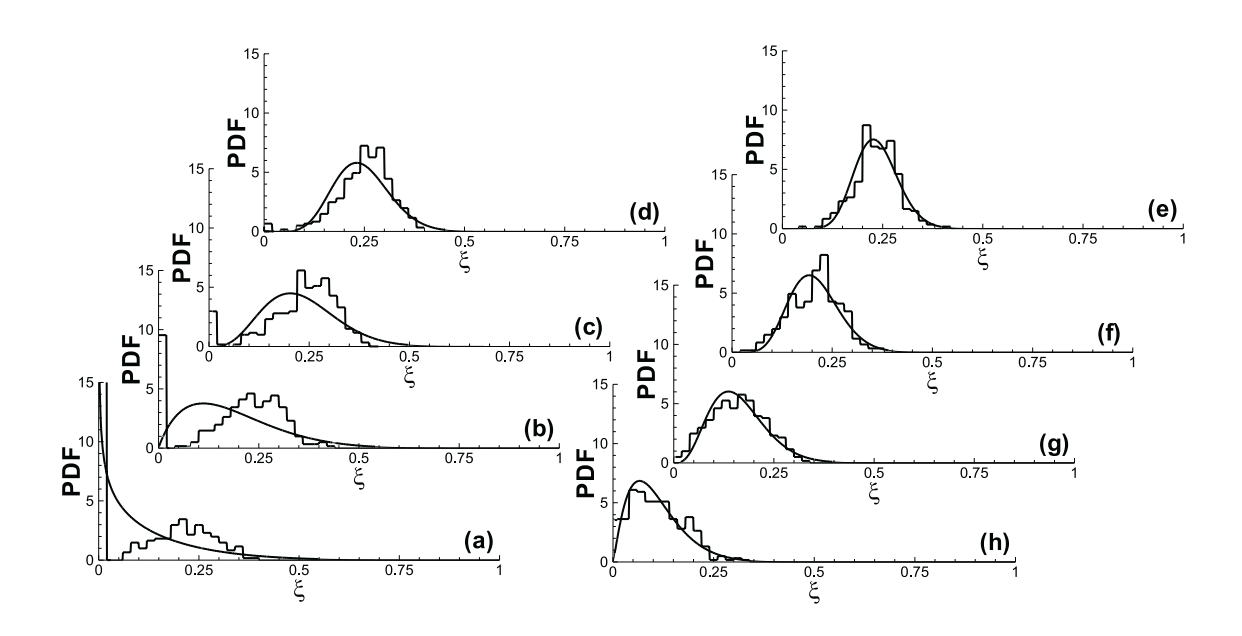


Figure 16. Measured concentration PDF (step-wise curve) and the calculated β -PDF (smooth curve) at the eight sampling points (positions shown in Figure 13) along the line perpendicular to the jet centerline at x=2.0rd.